Hydrology and Earth System Sciences Discussions

Skewness as measure of the invariance of instantaneous renormalized drop diameter distributions 2. Orographic precipitation

M. Ignaccolo[1] **and C. De Michele**[1]

[1]DIIAR, Politecnico di Milano, Milano, Italy

HESSD

8, 8101–8130, 2011

Comparison of drop size distributions

M. Ignaccolo and
C. De Michele

Title Page

Abstract | Introduction

Conclusions | References

Tables | Figures

◄ | ►

◄ | ►

Back | Close

Full Screen / Esc

Printer-friendly Version

Interactive Discussion

M. Ignaccolo and
C. De Michele

Full Screen / Esc

Printer-friendly Version

Interactive Discussion

Abstract

Here we use the *skewness* parameter, and the procedure developed in the companion paper (Ignaccolo and De Michele, 2011), to investigate the variability of instantaneous renormalized spectra of drop diameter in presence of orographic precipitation. Disdrometer data, available at Bodega Bay and Cazadero, California, are analyzed either as whole, or as divided (using the bright band echo) in precipitation intervals weakly and strongly influenced by orography, and compared to results obtained at Darwin, Australia. We find that also at Bodega Bay and Cazadero exists a most common distribution for the instantaneous renormalized spectra. The skewness values associated with the most common distributions are larger than those found at Darwin. No appreciable differences are found in the skewness distributions of precipitation weakly and strongly influenced by orography. However the renormalized drop diameter spectra of precipitation with strong orographic component have fatter right tail than precipitation with a weaker orographic component. The differences between orographic and non-orographic precipitation are investigated within the parametric space represented by number of drops, mean value and standard deviation of drop diameter. A filter is developed which is able to identify 1 min time intervals during which precipitation is mostly of orographic origin.

1 Introduction

Stratiform and convective are the two main categories used to describe rainfall. They indicate the strength (convective indicating the stronger case) of the updraft motion generating atmospheric vapor condensation and eventually rainfall drops (Houze, 1997). This categorization does not include explicitly the orography: the interaction between the land surface and the atmosphere. Mountains, and to a less degree hills, generally induce an uplift motion which may produce condensation and then precipitation (Roe, 2005). One of the most important effects due to orography is the so called

"orographic enhancement": the total amount of rainfall on the slopes of mountains and hills is larger than that on the surrounding planes. However the focus of this manuscript will be the effect of orography on the shape of drop diameter distributions regardless of any effect on cumulated rainfall rates.

In the present manuscript we consider data sets from three different sites. (1) Darwin (DRW), Australia, (2) Bodega Bay (BBY), California, USA, (3) Cazadero (CZD), California, USA. Darwin is on the coast backed by plains and it can be safely assumed the land surface "influence" on rain (intended as disturbance on rainfall rates, drop size distributions, and all the possible features of the rainfall phenomenon) to be negligible. This data set is the same one used in the companion paper "Skewness as measure of the invariance of instantaneous renormalized drop diameter distributions 1. Convective vs. stratiform precipitation". Bodega Bay is located on the coast of California, ~120 km North of San Francisco, while Cazadero is 10 km inland, 33 km Northwest of Bodega Bay. Immediately west of Bodega Bay are located the Coastal Range Mountains of California where Cazadero is at 475 m a.s.m.l. (all peaks in the region surrounding Bodega Bay and Cazadero are below 1000 m of altitude). At BBY and CZD the land surface influence on precipitation can be relevant. As matter of fact it has been observed that winter stratiform storms at these sites may lack the characteristic bright band echo signature for extensive period of times (White at al., 2003; Martner et al., 2008). During these time intervals, precipitation "is primarily the result of orographically forced condensation and coalescence processes" Martner et al. (2008).

It is important to stress that the distinction between time intervals where the bright band echo is present (BB intervals) versus those in which it is absent (NBB intervals) is done averaging 30 min radar data, and it must not be intended as a clear cut distinction between not orographic versus orographic rain ("BB and NBB rain often occurs in superposition" (Martner et al., 2008)) but more as the predominance of one mechanism of drop formation over another: BB mostly stratiform and NBB mostly orographic. The coastal range mountains in BBY and CZD can always induce condensation and coalescence of water droplets. Therefore the mere presence of the bright band signature

does not imply automatically the absence of precipitation of orographic origin. Conversely, the absence of the bright band signature does not automatically implies that aggregation of snow/ice crystal (the typical mechanism of drop production of stratiform rain) is absent but that (1) it is not so widespread for the melting of snow/ice crystal
5   to produce a strong bright band echo, (2) it is not predominant with respect to the precipitation of orographic origin.

The main purpose of this manuscript is to investigate the variability of the instantaneous (1 min sampling interval) renormalized spectra, in orographic precipitation, making use of the skewness. In the companion paper we have investigated the variability
10   at Darwin for the entire dataset and the stratiform and convective subsets. Hereby this investigation is repeated for Bodega Bay and Cazadero datasets in their entirety and dividing each of these in two subsets: BB (bright band echo present) and NBB (bright band echo absent). Moreover a comparison is made between the results at Darwin and those at Bodega Bay and Cazadero.

15   As in the companion paper, we divide each dataset in subsets of comparable values of skewness: skewness classes. For each skewness class subset, we compare the renormalized spectra for BB and NBB rain periods. While in Darwin stratiform (BB) and convective (NBB) precipitation have the same renormalized spectra, this is not true for Bodega Bay and Cazadero as NBB 1 min time intervals have fatter right tail
20   with respect to BB 1 min time intervals. Prior to renormalization instantaneous NBB spectra are much steeper than BB spectra. We this property to build a steepness-orographic filter which is able to identify 1 min time intervals during which precipitation is mostly orographic in origin: steep time intervals. Removing steep time intervals from the NBB data sets removes the discrepancies between the renormalized spectra of BB
25   and NBB skewness classes subsets.

Title Page

Abstract | Introduction

Conclusions | References

Tables | Figures

◄◄ | ►►

◄ | ►

Back | Close

Full Screen / Esc

Printer-friendly Version

Interactive Discussion

2   Data and methods

Hereby we summarize the data processing and methods adopted in our analysis. Most of these are the same as those used in the companion paper, in which case we present only a "quick" summary (the interested reader will find in the companion paper all the details), while new methods will be described in detail.

2.1   Data

We use Joss Waldvogel RD80 disdrometer data at 1 min time resolution from three different locations (1) Darwin (DRW) , Australia (12.45° S, 130.83° E, 2 m a.m.s.l.), (2) Bodega Bay (BBY), CA, USA (38.32° N, 123.07° W, 12 m amsl), (3) Cazadero (CZD), CA, USA (38.61° N, 123.21° W 475 m a.m.s.l.). For all datasets the drop diameters are classified in 20 different classes covering the range 0.3–5.6 mm, and 1-min counts are corrected against the instrument dead time Sauvageot and Lacaux (1995). The Darwin data set is the same of the companion paper. It consists of 97 consecutive days of measurements, from 4 November 2005 to 10 February 2006. Reflectivity maps are available for the time intervals 9 November to 6 December 2005, and 6 January to 10 February 2006, allowing for stratiform versus convective classification through the identification of the bright band. A total of 19 stratiform and 33 convective time intervals were identified with this method (see the online material in Ignaccolo and De Michele (2010)). The BBY data set consists of 1 min disdrometer counts for 100 non consecutive days spanning the 2003/2004 winter season from 6 December to 25 March. The CZD data set consists of 1 min disdrometer counts for 375 non consecutive days covering the winter seasons from year 2003 to 2006. Winter maritime storms at BBY and CZD are stratiform in nature. However radar data collected during these storms have shown that the "bright band" echo, which is characteristic of stratiform precipitation, is missing during extended period of times, not only at BBY and CZD, but on other locations in the Pacific North American coast as well (Neiman et al., 2005). The lack of the bright band has been associated (White at al., 2003; Martner et al., 2008)

to time intervals of hydrometeor growth primarily result of condensation and coalescence of water droplets in a relatively shallow layer near the surface: a mechanism of orographic origin (Kingsmill et al., 2006). From the BBY data set and the 2003/2004 winter part of the CZD database, we consider time intervals where the bright band is present (BB) and time intervals where the bright present is absent (NBB) following the classification scheme of Table I of Martner et al. (2008). In this way the subsets BBY-BB, BBY-NBB, CZD-BB, and CZD-NBB are obtained.

These data are processed as in the companion paper. Firstly minutes with total counts <60, or with only 2 diameter classes with non zero counts, are eliminated from the database. This procedure ensure that mean, standard deviation and other variables used to describe instantaneous distributions are statistically significant. After this procedure the remaining 1 min intervals are checked for outliers drop counts. Outliers drop counts occur when gaps (disdrometer classes with zero counts) exist between occupied diameter classes. For each minute we identify the class with the maximum count, and then the no gap region containing it. Drop counts which do not belong to the no gap region constitute a extremely small portion of the database (~0.1–0.2 % of the total number of drops) but could heavily influence the estimation of higher moments of the distribution, and thus these drop counts are set to zero. After this processing, the three data sets considered in this manuscript and their subsets have the following composition. (1) DRW 6863 min and 2753796 drops, DRW stratiform 1844 min and 354743 drops, and DRW convective 1536 min and 1064561 drops. (2) BBY 10804 min and 5389240 drops, BBY-BB 3273 and 1493843 min, BBY-NBB 2614 min and 1517381 drops. (3) CZD 76137 min 44252384 drops, CZC-BB 3883 min and 2006234 drops, and CZC-NBB 3551 min and 2887789 drops.

2.2 Methods

We adopt the same renormalization procedure of the companion paper. For each renormalization time interval I, 1 min in our case:

$$\begin{cases} D \to D_R = \dfrac{D - \mu_I}{\sigma_I} \\ p_{G,I}(D) \to p_{G,I}(D_R) = \sigma_I p_{G,I}(\sigma_I D_R + \mu_I) \end{cases} \qquad (1)$$

where μ_I and σ_I are the mean, and standard deviation of the drop diameter observed at the ground. This renormalization, originally introduced in (Ignaccolo et al., 2009; Ignaccolo and De Michele, 2010), operates differently from the other renormalizations available in Literature, e.g. (Willis, 1984; Sempere Torres et al., 1994; Maki et al., 2001; Testud et al., 2001; Uijlenhoet et al., 2003; Campos et al., 2006; Hazenberg et al., 2011). In fact Eq. (1) operates a change of variable, from the drop diameter D to the renormalized diameter D_R, having zero mean and unit variance. The instantaneous renormalized spectrum is, in this case, the instantaneous probability density $p_{G,I}(D_R)$ of the renormalized drop diameter. This density is obtained from that of the drop diameter observed at the ground $p_{G,I}(D)$ using the second identity of Eq. (1).

Usually disdrometer data are categorized in diameter classes so that for each drop one does not know the "exact" value of the diameter, but only that the diameter was in a given range. We refer to this effect as the "quantization error". Due to the quantization error the probability density $p_{G,I}(D)$, and as a consequence the probability density $p_{G,I}(D_R)$, is a step function with constant value inside the range of each diameter class. Moreover given a series of disdrometer counts, it is not possible to associate to it an unique series of renormalized diameter D_R. However one can associate to a disdrometer count n_j of the j-th class, n_j different diameter values of D extracted randomly and uniformly in the range of j-th class, and using the first identity of Eq. (1) n_j different values of the renormalized drop diameter D_R. With this process of "randomization", one can associate to a sequence of disdrometer drop counts a sequence of renormalized drop diameters, and then a density $p_G^{\text{rand}}(D_R)$. Each repetition of the randomization

8107

process creates a new sequence and a new density. In the limit of an infinite number of repetitions the arithmetic average of the densities $p_G^{rand}(D_R)$ converges to a limiting distribution $p_G(D_R)$:

$$p_G(D_R) = \frac{1}{N} \sum_l N_l \, p_{G,l}(D_R) \qquad (2)$$

where N_l is the drop count in the l-th renormalization time interval, $p_{G,l}(D_R)$ is the instantaneous renormalized spectrum, and N is the total number of drops in the particular sequence of disdrometer drop counts considered. We consider the probability density $p_G(D_R)$ defined by Eq. (2) as the renormalized spectrum associated with a particular series of disdrometer drop counts.

As in the companion paper, the skewness is used to compare instantaneous renormalized spectra $p_{G,l}(D_R)$ and the concept of skewness class will be used to divide a data set in subsets with comparable values of skewness. A renormalization time interval l belongs to the skewness class r if the relative difference of the corresponding skewness γ_l with respect the most probable value 0.64 is within the percentage range $[(r - 1/2) \times 100, (r + 1/2) \times 100]$: e.g. the skewness class zero (s0) implies γ_l in the range [0.32, 0.96], the skewness class plus-one (s+1) implies γ_l in the range [0.96, 1.60], while the skewness class minus-two (s-2) implies γ_l in the range [−0.96, −0.32].

2.2.1 Additional parameters used to describe drop size distributions

Additional parameters are used to characterize the properties of the instantaneous spectra. The kurtosis κ_l will be used in addition to the skewness γ_l to characterize renormalized instantaneous spectra $p_G^l(D_R)$. Note that the kurtosis and in general all standardized moments of order ≥ 3 are left unchanged under the renormalization procedure adopted in this manuscript (see companion paper). In addition to the kurtosis we will describe the properties of the not renormalized instantaneous spectra $p_G^l(D)$ using (1) The disdrometer diameter class of maximum density $J_{m,l}$: the modal class.

Full Screen / Esc

Printer-friendly Version

Interactive Discussion

(2) The class span S_l: the number of consecutive disdrometer diameter classes with non zero probability density. (3) The percentage occupancy $\%O_l$: the fraction ($0 \to 1$) of the probability density contained in the first four disdrometer diameter classes. (4) The left and right gradients $\nabla_{L,l}$ and $\nabla_{R,l}$ of the probability density around the maximum value. These last quantities are defined as follows:

$$\begin{cases} \nabla_{L,l} = \dfrac{p_{G,l}(D_{j_{m,l}-k}) - p_{G,l}(D_{j_{m,l}})}{D^R_{j_{m,l}} - D^L_{j_{m,l}-k}} \\[2em] \nabla_{R,l} = \dfrac{p_{G,l}(D_{j_{m,l}+k}) - p_{G,l}(D_{j_{m,l}})}{D^R_{j_{m,l}+k} - D^L_{j_{m,l}}} \end{cases} \tag{3}$$

where $D_{j_{m,l}}$ is the middle value of the $j_{m,l}$ diameter class, while the symbol D^L_l (D^R_l) indicates the left (right) border of the l diameter class. The integer k is set to 4 unless $p_{G,l}(D_{j_{m,l}\pm4})$ is equal to zero or $j_{m,l}\pm4$ is not a valid value ([1,20]) for a diameter class. In such a case k is set to the maximum possible value in the range [0,3] so that $p_{G,l}(D_{j_{m,l}\pm4})$ is larger than zero or $j_{m,l}\pm4$ is a valid value for a class diameter: e.g. if $j_{m,l} = 0$ than $k = 0$ and $\nabla_{L,l} = 0$. The smaller is the value of the gradients defined in Eq. (3) the steeper is the distribution.

3 Results

3.1 Skewness

Figure 1 shows the probability $Pr(\gamma_l)$ of having a renormalized (not renormalized) spectrum $p_{G,l}(D_R)$ ($p_{G,l}(D)$) with skewness γ_l for all the datasets examined: DRW database and its two subsets, stratiform and convective, on the top panel, BBY and its two subsets, BBY-BB and BBY-NBB, on the middle panel, and CZD and its two subsets, CZD-BB and CZD-NBB, on the bottom panel. The results in Bodega Bay and Cazadero

mirrors those in Darwin. In all cases the probability $Pr(\gamma_l)$ for the entire datasets (full lines) is strongly peaked. In all cases the distributions relative to subsets with a bright band signature (DRW stratiform, BBY-BB, and CZD-BB) and to those without a bright band signature (DRW convective, BBY-NBB, and CZD-NBB) are similar to each other and to the results for the entire datasets. The main difference is in the locations of the peaks, the distributions in Darwin are peaked at $\gamma_l \simeq 0.64$, those in Bodega Bay at $\gamma_l \simeq 0.72 - 0.88$, and those in Cazadero at $\gamma_l \simeq 0.88 - 1.04$. We will propose a possible explanation for the origin of the shift in the peak location in the "Conclusions" Section.

Table 1 reports, for the bright band and not bright band subsets at Bodega Bay and Cazadero, the percentages $l\%$ of the renormalization time intervals in the data set belonging to a given skewness class, and the percentage $d\%$ of the database total number of drops belonging to renormalization time intervals in a given skewness class. As expected from Fig. 1, the percentage $l\%$ inside each skewness class does not change appreciably between BB and NBB subsets in the same location, the only notable differences are $\sim +5\%$ difference in the population of the s0 skewnwss class, and $\sim -4\%$ in the population of the s+2 skewness class between CZD-BB and CZD-NBB. More notable differences occur if one considers the $d\%$ of drops inside each skewness class. In this case when moving from the BB to the NBB subset the percentage of drops in the skewness class s0 increases ($\sim +7.5\%$ for BBY and $\sim +10\%$ for CZD) and that in the skewness class s+2 decreases ($\sim -2.5\%$ for BBY and $\sim -6.5\%$ for CZD).

3.2 Renormalized spectra of skewness classes data sets

Next, we divide, as done in the companion paper, all databases in subsets according to the skewness class of each renormalization time interval. We calculate the probability density $p_G(D_R)$ of the renormalized drop diameter D_R for each subsets using Eq. (2). Figure 2 depicts the results for the skewness classes from −2 to +3 (the remaining skewness classes have to few $\lesssim 10$ time intervals in the corresponding data sets and are not considered for comparison) for the entire DRW data set (solid line), BBY-BB (long dashed line) and BBY-NBB (circles) subsets, and CZD-BB (short dashed line)

and CZD-NBB (triangle) subsets. For the Darwin site no distinction is done between stratiform and convective since no appreciable difference exists in this case (see Fig. 3 of the companion paper). We see how the results for the BBY-BB and CZD-BB are similar to those of the Darwin data sets for all the skewness classes. Some differences are observed for the s+3 skewness class where DRW, BBY-BB, and CZD-BB densities have the same shape until the DRW and then the BBY-BB densities drop sharply. These differences are due to sampling inaccuracies and are not statistically significant. We consider the range for which densities are statistically signficant as the range for which the density values correspond to probability values $\geq 10/M$, M being the total number of drops in the data set considered. When the densities $p_G(D_R)$ of NBB subsets are compared to BB subsets we see how a fatter left tail is present for the s0, s+1, and s+2 skewness classes. These differences cannot be ascribed just to sampling effects. On the contrary, the fatter left tails for the s+3 class, and the lack of an extended right tail for the s-1 and s-2 clsses are due to sampling inaccuracies.

Figure 2 indicates that the main differences between the densities $p_G(D_R)$ of the renormalized drop diameter D_R relative to the BB and NBB subsets both at Bodega Bay and at Cazadero occur for the skewness class s0, s+1, and s+2. Since during time intervals without bright band signature precipitation is mostly orographic in nature (Martner et al., 2008), the observed differences must be due to peculiar properties of the shape of instantaneous spectra of orographic origin. These properties are evidently not "captured" by the skewness parameter since Fig. 1 indicates that there are no relevant differences in the distribution of skewness values for the BB and NBB rain in both Bodega Bay and Cazadero sites. Is/Are there a/some parameter/s other than the skewness which can be used to "capture" the BB vs NBB discrepancies?

3.3 Differences in spectra between BB from NBB precipitation

We will now look for parameters describing instantaneous spectra, $p_{G,I}(D)$, to build a metric which somewhat separates bright band from not bright band rain time intervals at Bodega Bay and Cazadero. In order to avoid presenting the results of the following

analysis for the s0, s+1 and s+2 classes separately, we pasted together the s0, s+1, and s+2 subsets creating the s012 skewness class subset for each one of the data base we considered: s012-BBY-BB, s012-BBY-NBB, s012-CZD-BB, s012-CZD-NBB, s012-DRW stratiform, and s012-DRW convective (we did split the Darwin data set so that we can directly compare bright band data sets at Bodega Bay and Cazadero with stratiform precipitation in absence of any orographic effect as we expect to be the case in Darwin). Results relative to s012 subsets do not differ for all practical purpose from those relative to single skewness classes (s0, s+1, and s+2) subsets. In all the figures presented, lines will indicate the results for s012 subsets with a bright band signature (solid line for s012-DRW stratiform, long dashed line for s012-BBY-BB, and short dashed lines for s012-CZD-BB dataset), while points indicate the results for data sets without a bright band signature (squares for s012-DRW convective, circles for s012-BBY-NBB, triangles for the s012-CZD-NBB).

3.3.1 Kurtosis

The next logical choice after the skewness γ_l, in our analysis' scheme, to describe the properties of instantaneous spectra is the kurtosis k_l: the fourth standardized moment. In the top-left panel of Fig. 3 we plot the cumulative distribution functions $\mathcal{F}(\kappa_l)$ of the kurtosis. No relevant differences are observed between bright band and not bright band cumulative distributions. In this sense we judge the kurtosis to not be a valid metric to "separate" BB and NBB data sets at Bodega Bay and Cazadero. We notice how the kurtosis values grow larger moving from Darwin to Bodega Bay and then to Cazadero. This growth is simply due to the growth in skewness (shift of the peak location of $Pr(\gamma_l)$) shown in Fig. 1) as the skewness value "fixes" also the kurtosis value. To prove this point we consider the range [0.32, 2.24] of skewness values (the entire range of the s0, s+1, and s+2 skewness classes) and divide it in bins of width 0.16 (1/4 of the range of a skewness class). For each bin we consider all the possible values of the kurtosis and calculate the 5 %, 50 %, and 95 % percentile of the corresponding distributions. We see, top-right panel and bottom panels of Fig. 3, how the 5 % and 50 % are really

indenpendent from the particular data sets considered. The same can be said for the 95 % althought the results are more "noisy" as they are partially affected by statistically inaccuracies. In this sense, the skewness γ_I "determines" the kurtosis κ_I not depending on site location or presence/absence of a bright band radar echo.

3.3.2 Other parameters

Next, we consider other possible parameters describing the instantaneous spectra in order to differentiate between BB and NBB rain periods. These parameters are (see Sect. 2.2.1) the disdrometer diameter class of maximum density $J_{m,I}$, the class span S_I, the percentage occupancy $\%O_I$, the left and right gradients $\nabla_{L,I}$ and $\nabla_{R,I}$ of the probability density around the maximum value. Figure 4 illustrates the cumulative density functions for these variables. When we compare NBB result at Bodega Bay and Cazadero with the corresponding BB at the same sites, we see how NBB instantaneous probability densities $p_{G,I}(D)$ are more concentrated on the first four diameter classes $\Rightarrow D \leq 0.715$ mm ($\mathcal{F}(\%O_I)$), are narrower ($\mathcal{F}(S_I)$), and have the maximum located predominantly (>90 % of the cases) in the first 4 diameter class ($\mathcal{F}(j_{m,I})$). These observed properties closely match the known properties of orographic precipitation: drop size distributions which have an abundance of small drops, and are narrow, with the largest diameters rarely exceeding 2 mm (Blanchard, 1953; Fujiwara, 1967). We note also how the discrepancies between NBB and BB are consistently larger in Cazadero than in Bodega Bay. Next we compare the cumulative density functions $\mathcal{F}(\%O_I)$ and $\mathcal{F}(j_{m,I})$ for the s012-BBY-BB and s012-CZD-BB data sets with to those relative to the s012-DRW stratiform data set. At Bodega Bay and Cazadero the max value of density is more likely to occurr in the first four class which also contain a larger fraction of the total density. Again at Cazadero the discrepancies are larger than at Bodega Bay. Moreover, the s012-BBY-BB and s012-CZD-BB are closer to the s012-DRW stratiform line than the s012-BBY-NBB and s012-CZD-NBB curves. These reduced discrepancies are compatible with the notion that even if the bright band signature is present same precipitation which is orographic in nature may still occur (Martner et al., 2008).

Regarding the span S_I we observe a slightly larger (smaller) average value for the s012-BBY-BB (s012-CZD-BB) data set when compared to the Darwin stratiform data set. Finally the results relative to DRW convective data set show that convective precipitation with respect to stratiform precipitation has on average a larger span S_I, but comparable percentage occupancy %O_I and disdrometer diameter class of maximum density $J_{m,I}$.

The bottom panel in Fig. 4 shows the cumulative density functions for the left and right gradients $\nabla_{L,I}$ and $\nabla_{R,I}$ of the instantaneous probability density $p_{G,I}(D)$ around the maximum value. The horizontal solid line indicates the 5 % probability level, while the vertical line the zero value for both the left and right gradients. The right gradients of NBB databases at Bodega Bay and Cazadero have much smaller ($\simeq 4$ times smaller) 5 % percentile and wider range (0 to minimum value) than the corresponding BB data bases. Among data sets with a bright band s012-BBY-BB and s012-CZD-BB have a much wider ($\simeq 3$ time larger) range than the DRW stratiform data set, however the 5 % percentile of s012-BBY-BB is almost identical to DRW stratiform, while that of s012-CZD-BB is almost the double. In all cases, databases at Cazadero have the smallest 5 % percentile. For the left gradients both s012-BBY-NBB and s012-CZD-NBB have a smaller (-60 % and -70 % resepctively) 5 % percentile than s012-BBY-BB and s012-CZD-BB. The range of s012-BBY-NBB is wider than those of s012-BBY-BB but the opposite is true for s012-CZD-NBB and s012-CZD-BB. Moreover the data sets in Bodega bay are those with the smallest 5 % percentile. This is due to the fact that for $\gtrsim 60$ % of the s012-CZC-NBB data set the disdrometer diameter class of maximum density $J_{m,I}$ is the first one $\Rightarrow \nabla_{L,I} = 0$, with second third and fourth classes having a much smaller probability. However for the s012-BBY-NBB the most probable disdrometer diameter class of maximum density $J_{m,I}$ is the second class followed by the third and the by the first (≤ 20 %). As a consequence there are many more $\nabla_{L,I} < 0$ for s012-BBY-NBB than for s012-CZD-NBB. For data sets with a bright band signature, the s012-DRW stratiform dataset and the s012-BBY-BB have almost identical left gradients, while the s012-CZD-BB value is larger by a factor 0.5. The range is also the

Full Screen / Esc

Printer-friendly Version

Interactive Discussion

widest for s012-DRW stratiform, with s012-BBY-BB and s012-CZD-BB having both $\simeq$ 20 % smaller ranges. Finally both for the right and left gradients the 5 % percentile and the range of the s012-DRW convective data set is similar to that of the s012-DRW stratiform data set.

3.4 Steepness filter

The division in BB versus NBB sets according to radar maps is not a "black vs white" one. Radar maps are obtained averaging 30 min echoes data, while instantaneous distributions refer to 1 min time intervals. Thus during BB (NBB) intervals is possible the presence of 1 min time intervals for which precipitation is almost exclusively of oro-graphic (stratiform) origin. Even more complicated situations can arise are both the orographic and stratiform mechanisms of drop production can operate simultaneously with different relative strength. Hereby, we look for a metric which is capable of iden-tifying 1 min time intervals where precipitation occurred mainly through an orographic mechanism. One of the advantages of this eventual metric with respect to the radar echoes used by Martner et al. (2008) would be its 1 min time resolution versus the 30 min resolution of the radar technique. The results of Fig. 4 indicate that a sharp difference exists between NBB and BB data sets at Bodega Bay and Cazadero for the right and left gradients. Therefore we use this variable to build a "steepness-orographic filter". One could envision a different metric, however the proposed metric has, in our opinion, some remarkable properties.

Given a renormalization time interval I (of length 1 min in our case) of a dataset belonging to either the s0, s+1, or s+2 skewness classes, the steepness-orographic filter operates as follows

$$
\begin{cases}
I \text{ is steep if} & \nabla_{L,I} \leq -9.2 \quad \text{OR} \quad \nabla_{R,I} \leq -4 \\
I \text{ is not steep if} & \nabla_{L,I} > -9.2 \quad \text{AND} \quad \nabla_{R,I} > -4
\end{cases}
\tag{4}
$$

The values -9.2 and -4 are the 5 % percentile of the left and right gradients for the

DRW stratiform dataset. Thus this filter labels as "of strong orographic nature" the precipitation inside all renormalization time intervals whose left and right gradients qualify as statistically "uncommon" (5 % percentile) at Darwin (which is taken as reference data set for absence of orographic effect). When applied to the s012-BBY-NBB data set, 1428/2325 ($\simeq$ 61.41 %) renormalization time intervals are classified as steep, while for the CZD-NBB data set the ratio is 2381/3213 ($\simeq$74.10 %). For the data sets with bright band signature we find a ratio of 251/3004 ($\simeq$8.35 %) for BBY-BB, and of 1149/3492 ($\simeq$ 32.90 %) for CZD-BB.

We now consider where the steep and not-steep portions of a dataset reside in the $\log_{10}(N_l)\mu_l\sigma_l$-plane. The average μ_l and the standard deviation σ_l of the drop diameters are the only two parameters involved in the renormalization procedure, Eq. (1). While the drop count N_l is the inverse of the average precipitation rate (the logarithm of the drop count for achieve a better visualization). These three parameters are the "main" variables adopted in our statistical description of the rainfall phenomenon: e.g. we have shown in Ignaccolo and De Michele (2010) that rainfall rate classes (Tokay and Short, 1996) occupy almost non overlapping volumes in the $\log_{10}(N_l)\mu_l\sigma_l$-plane. One remarkable property of the steepness filter is that the steep and not-steep portions of a data base (s012-BBY-NBB, s012-BBY-BB, s012-CZD-NBB, and s012-CZD-BB in our case) occupy two non overlapping volumes in the $\log_{10}(N_l)\mu_l\sigma_l$-plane. The $\mu_l\log_{10}(N_l)$-plane projections, left colum of Fig. 5, indicate that no not-steep (blue crosses) renormalization time intervals have an average diameter $\mu_l \lesssim 0.5$ mm, while steep renormalization time intervals (red squares) are mostly concentrated in the region $\mu_l \lesssim 0.5$ mm although some have a larger value of the average diameter. This overlap between steep and not-steep intervals is not present in the $\mu_l\sigma_l$-plane projections, right column of Fig. 5, where red squares and blue crosses desing two matching puzzle pieces: steep renormalization time intervals with an average diameter $\mu_l \gtrsim 0.5$ mm have a standard deviation σ_l which is either larger or smaller than that of not-steep diameter indicating a "strong correlation" between μ_l, σ_l and the "steepness' of the instantaneous probability density $p_{G,l}(D)$.

Another remarkable property of the steepness-orographic filter is that it eliminates the right fatter tail discrepancies for the probability density $p_G(D_R)$ of the renormalized drop diameter D_R, Eq. (2), observed in Fig. 2 in the case of the s0, s+1, and s+2 skewness class substes of NBB rain periods. Fig. 6 shows, left columns, probability densities $p_G(D_R)$ for the skewness class s0, s+1, and s+2 sub sets of the not-steep portions of the s012-BBY-NBB and s012-CZD-NBB data sets, together with the corresponding densities for BBY-BB and CZD-BB. There are no fatter tails and the densities are remarkably similar. Although s012-BBY-BB and and s012-CZD-BB have steep renormalization time interals their contribution to the tails is not relevant and their inclusion or not does not alter the densities. If we compare the densities BBY-BB and CZD-BB with the steep portions of the s012-BBY-NBB and s012-CZD-NBB data sets, right column of Fig. 6, we see again the right fatter tail discrepancies.

It may seems counterintuitive that steeper distributions result in a fatter tail. However it is not so. The left and right gradient $\nabla_{L,I}$ and $\nabla_{R,I}$ are defined for the instantaneous probability density $p_{G,I}(D)$ while the fatter right tail occurs for $p_G(D_R)$ which is an average, Eq (2), of single instantaneous renormalized density $p_{G,I}(D_R)$. The left and right gradients are not preserved by the renormalization procedure. Using Eq. (1) together with Eq.(3) we see that the left and right gradients for the densities $p_{G,I}(D_R)$ differ from those relative to $p_{G,I}(D)$ by a multiplicative factor $(\sigma_I)^2$. Steep renormalization time intervals have a less than unity standard deviation, and have a smaller standard deviation than not-steep renormalization time intervals, with the exception of a fraction of the cases for which $\mu_I \gtrsim 0.5\,\text{mm}$ (Fig. 5). Therefore the steepness of $p_{G,I}(D_R)$ is greatly reduced for steep, according to $p_{G,I}(D)$, renormalization time intervals while, in comparison, not-steep, according to $p_{G,I}(D)$, renormalization time intervals are subject to a much smaller reduction. A similar effect would be expected for the left tail, at least in the case of the BBY-NBB subsets as suggested by the cumulative density function $\mathcal{F}(\nabla_{L,I})$, bottom panel of Fig. 4. However fatter left tails are not observed for the density of the BBY-NBB, or any other subsets. The rationale is that (1) overall the value of the left gradients are larger (less steep) than those of the right gradients. (2) Very small

values of the left gradients occur for 1 min time intervals for which the maximum of the density $p_{G,I}(D)$ and the mean values μ_I (see Figs. 4 and 5) are located predominatly in the first four diamter classes. As a consequence extremely negative values of the renormalized drop diameter, see Eq. (1), do not occur.

⁵   Finally, we see how the division in steep and not-steep subsets affects the cumulative density functions of the disdrometer diameter class of maximum density $J_{m,I}$, the class span S_I, the percentage occupancy %O_I, Fig. 7 reports on the left column the results for the s012-BBY-BB ans s012-CZD-BB data sets, and on the right column the results for the s012-BBY-NBB and s012-CZD-NBB data sets. We see how in all cases the steep

¹⁰ subsets (red and blue solid lines with not filled points) have instantaneous spectra which are more concentrated in the first four diameter classes, more narrow, and more apt to have a maximum in the first four diameter classes than the entire data sets (red and blue solid lines): in this sense the figure validates the use of the word "orographic" in "steepness-orographic filter. Not-steep subsets (red and blue solid lines with filled

¹⁵ points) have instantaneous spectra whose properties are closer to those of the DRW stratiform batabase (solid black line).

4   Conclusions

The results presented in this manuscript can be summarized as follows.

    Both in Bodega Bay and in Cazadero the distribution $Pr(\gamma_I)$ of skewness value of

²⁰ instantaneous spectra is strongly peaked (Fig. 1). Thus there is a most common distribution as in the case of Darwin explored in detail in the companion paper. As for Darwin there are no drammatics differences in $Pr(\gamma_I)$ between data sets with or without a bright band signature, even if the absence of a bright band echo in Darwin is indicates the occurrence of convective precipitation, while in Bodega Bay and in Cazadero the

²⁵ occurrence of orographic precipitation.

    Differences are present for the renormalized spectra $p_G(D_R)$ relative to different skewness classes subsets of bright band and not bright band rain periods (Fig. 2).

In the latter case the subsets relative to the skewness classes s0, s+1, and s+2 have a fatter right tail. These differences are not present in Darwin when one compares stratiform (bright band) to convective (no bright band) precipitation. In Darwin stratiform or convective instantaneous renormalized spectra with the "same" (in the sense of skewness class) value of skewness have a common shape. This is not true in Bodega Bay and in Cazadero as NBB spectra differ from BB spectra in spite of having the same skewness.

NBB instantaneous spectra are, with respect to BB spectra, more concentrated in the first four diameter classes $D \leq 0.715$ mm, narrower, more apt to have the maxima located in the first for diameter classes, and are steeper: in accordance with the known characteristic of orographic precipitation (Blanchard, 1953; Fujiwara, 1967) and with the identification of NBB as rain periods during which condensation and precipitation are mostly orographic in nature (White at al., 2003; Martner et al., 2008).

We used the steepness parameters $\nabla_{L,I}$ and $\nabla_{R,I}$ to define a steepness-orographic filter which divides a data set in steep and not-steep subsets. A remarkable property of this filter is that steep and not-steep renormalization time intervals occupy two separate volumes in the $\log_{10}(N_I)\mu_I\sigma_I$-plane (Fig. 5). This means that one can redefine the steepness-orographic filter in terms of the parameters N_I, μ_I, and σ_I (since no appreciable overlap is observed between the steep and not-steep volume projections on the $\mu_I\sigma_I$-plane, one could redifine the steepness-orographic filter using in terms of μ_I and σ_I only). Another remarkable feature is that the filtering procedure eliminates the discrepancies (see Fig. 6) observed for renormalized spectra $p_G(D_R)$ relative to different skewness classes (s0, s+1, and s+2) subsets of bright band and not bright band rain periods.

It is worth clarifying in which sense the filter defined in Eq. (4) is an "orographic" filter. Renormalization time intervals denoted as steep are time intervals during which precipitation is almost exclusively of orographic origin (Figs. 4, 5, and 7). This does not mean that during not-steep time intervals orographic precipitation does not occur but just that it is not predominant.

Finally we want to comment on what may cause the shift on the location of the maxima of $Pr(\gamma_l)$ observed in Fig. 1. After all, bright band (stratiform) precipitation at Bodega Bay and Cazadero should have the same characteristic of that at Darwin. A possibility is that the difference in peak location is due to the fact that at Darwin the precipitation is of monsoonic origin while the data bases considered at Bodega Bay and Cazadero refer to winter storms arriving from the Pacific Ocean: synoptic conjecture. However, we think that the evidence presented here suggests another conjecture: the orographic conjecture. The shift may be due to the presence orographic precipitation. In fact even in the presence of the bright band signature (the presence of a bright band echo is inferred using 30 min averaged radar data) orographic precipitation may occurr and be either predominant leading to "steep" time intervals ($\simeq 8.35\%$ of BBY-BB and $\simeq 32.90\%$ of CZD-BB data sets are made of steep intervals) or simply occur in superposition, without being predominant, to the rain of stratiform origin (White at al., 2003; Martner et al., 2008). In the latter case we expect an enhacemnt of the drop population in the first four classes ($\%O_l$) and larger possibility that the maximum of instantaneous spectra to be located in the first four class ($j_{m,l}$), and the span (S_l) of the spectra to remain essentially inaltered. This is precisely what we observe when we compare (Figs. 4 and 7) the cumulative density functions for the variables O_l, $j_{m,l}$, and S_l of BB data set or not-steep subsets of any set with the respective cumulative density functions for stratiform precipitation at Darwin. Moreover the fact the Cazadero is in the Coastal Range Mountain, while Bodega Bay is on the coast would suggest a strong orographic effect in Cazadero than in Bodega Bay explaining why the shift in skewness values is larger at Cazadero.

References

Blanchard D. C.: Raindrop size-distribution in Hawaiian rains, J. of Meteorology, 10, 457–473, 1953. 8113, 8119

Campos E. F.: On measurements of drop size distribution, Top. Meteor. Oceanog., 6(1), 24–30, 1999.

Campos, E. F., Zawadzki, I., Petitdidier, M., and Fernandez, W.: Measurement of raindrop size distributions in tropical rain at Costa Rica, J. Hydrol., 328, 98–109, 2006. 8107

Fujiwara, M.: Raindrop size distribution in warm rain as measured in Hawaii, Tellus XIX, 3, 392–402, 1967. 8113, 8119

Hazenberg, P., Nan, Y., Boudevillain, B., Delrieu, G., and Uijlenhoet, R.: Scaling of raindrop size distributions and classification of radar reflectivity rain rate relations in intense Mediterranean precipitation, J. Hydrol., 402, 179–192, 2011. 8107

Houze, R. A.: Stratiform precipitation in regions of convection: a meteorological paradox?, Bull. Am. Meteorol. Soc., 78(10), 2179–2196, 1997. 8102

Ignaccolo, M., De Michele, C., and Bianco, S.: The drop-like nature of rain and its invariant statistical properties, J. Hydrometeorol., 10 (1), 79–95, 2009. 8107

Ignaccolo, M. and De Michele, C.: Statistical collapse of stratiform and convective drop diameter distributions at the ground, Geophys. Res. Lett., 37, L24402, doi:10.1029/2010GL045454, 2010. 8105, 8107, 8116

Joss, J. and Gori, E. G.: Shapes of raindrop size distributions, J. Appl. Meteorol., 17, 1054–1061, 1978.

Kingsmill, D. E., Neiman, P. J., Ralph, F. M., and White, A. B.: Synoptic and topographic variability of northern Cali- fornia precipitation characteristics in landfalling winter storms observed during CALJET, Mon. Weather Rev., 134, 2072–2094, 2006. 8106

Konstinski, A. B. and Jameson, A. R.: Fluctuation properties of precipitation. Part I: On Deviations of Single-Size Drop Counts from the Poisson Distribution, J. Atmos. Sci. 54, 2174–2186, 1997.

Maki, M., Keenan, T. D., Sasaki, Y., and Nakamura, K.: Characteristics of the raindrop size distribution in tropical continental squall lines observed in Darwin, Australia, J. Appl. Meteorol., 40, 1393–1412, 2001. 8107

Martner, B. E., Yuter, S. E., Allen, B. W., Matrosov, S. Y, Kingsmill, D. E., and Ralph, F. M.: Raindrop Size Distributions and Rain Characteristics in California Coastal Rainfall for Periods

with and without a Radar Bright Band, J. Hydrometeorol., 9(3), 408–425, 2008. 8103, 8105, 8106, 8111, 8113, 8115, 8119, 8120

Neiman, P. J., Wick, G. A., Ralph, F. M., Martner, B. E., White, A. B., and Kingsmill, D. E.: Wintertime nonbrightband rain in California and Oregon during CALJET and PACJET: Geographic, interannual and synoptic variability, Mon. Weather Rev., 133, 1199–1223, 2005. 8105

Roe, G. H.: Orographic precipitation, Ann. Rev. Earth Pl. Sci. 33, 645–671, 2005. 8102

Sauvageot, H. and Lacaux, J. P.: The Shape of Averaged Drop Size Distributions, J. Atmos. Sci., 52, 1070–1083, 1995. 8105

Sekhon, R. S. and Srivastava, R. C.: Doppler radar observations of drop-size distributions in a thunderstorm, J. Atmos. Sci., 28, 983–994, 1971.

Sempere Torres, D., Porrà, J. M., and Creutin, J. D.: A general formulation for raindrop size distribution, J. Appl. Meteorol. 33, 1494–1502, 1994. 8107

Smith, J. A.: Marked point process models of raindrop-size distributions, J. Appl. Meteorol., 32, 284–296, 1993.

Testud, J., Oury, S., Black, R. A., Amayenc, P., and Dou, X.: The concept of normalized distribution to describe raindrop spectra: a tool for cloud physics and cloud remote sensing, J. Appl. Meteorol., 40, 1118–1140, 2001. 8107

Tokay, A. and Short, D. A.: Evidence from tropical raindrop spectra of the origin of rain from stratiform versus convective clouds, J. Appl. Meteorol., 35(3), 355–371, 1996. 8116

Uijlenhoet, R., Smith, J. A., and Steiner, M.: The microphysical structure of extreme precipitation as inferred from ground-based raindrop spectra, J. Atmos. Sci., 60, 1220–1238, 2003. 8107

White, A. B, Neiman, P. J., Ralph, F. M., Kingsmill, D. E, Ola, P., and Persson, G.: Coastal Orographic Rainfall Processes Observed by Radar during the California Land-Falling Jets Experiment, J. App. Meteorol., 4(2), 264–282, 2003. 8103, 8105, 8119, 8120

Willis, P. T.: Functional fits to some observed dropsize distributions and parameterization of rain, J. Atmos. Sci., 41, 1648–1661, 1984. 8107
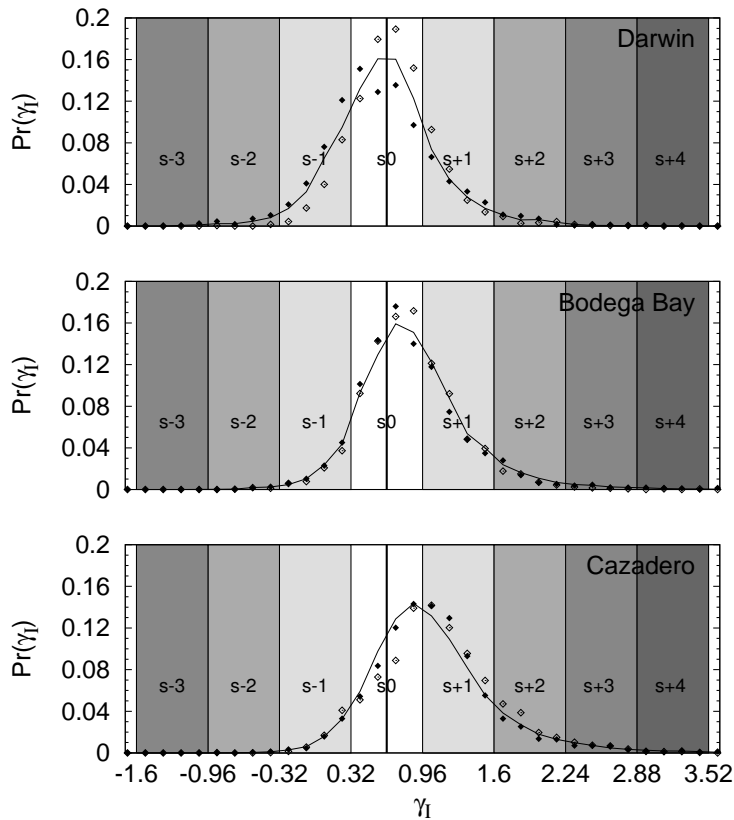
Title Page

Abstract | Introduction

Conclusions | References

Tables | Figures

|◄ | ►|

◄ | ►

Back | Close

Full Screen / Esc

Printer-friendly Version

Interactive Discussion

Table 1. Classification of the BBY-BB, BBY-NBB, CZD-BB, and CZD-NBB data sets in classes of skewness using the number of time intervals ($I\,\%$), and number of drops ($d\,\%$).

Data set		BBY BB		BBY NBB		CZC BB		CZC NBB	
Class of γ		$I\%$	$d\%$	$I\%$	$d\%$	$I\%$	$d\%$	$I\%$	$d\%$
s-2	[−0.96,−0.32]	0.33	0.21	0.42	0.18	0.05	0.009	0.25	0.05
s-1	[−0.32,0.32]	7.15	7.32	8.49	5.03	6.51	5.88	5.66	3.32
s0	[0.32,0.96]	57.28	53.92	56.04	61.57	35.17	33.89	40.13	43.38
s+1	[0.96,1.60]	30.09	29.82	27.54	25.84	42.72	41.21	41.87	42.51
s+2	[1.60,2.24]	4.40	7.51	5.35	4.90	12.02	14.05	8.47	7.46
s+3	[2.24,2.88]	0.58	0.80	1.22	1.20	2.83	3.98	2.29	2.17
s+4	[2.88,3.52]	0.12	0.34	0.46	0.54	0.46	0.63	0.59	0.53
s+5	[3.52,4.16]	0.03	0.06	0.34	0.54	0.12	0.20	0.50	0.44
s+6	[4.16,4.80]	0	0	0.04	0.07	0.08	0.12	0.08	0.09

Fig. 1. The probability $Pr(\gamma_I)$ for the datasets examined. In all panels, full lines indicate the probability for the entire dataset, white diamonds the probability for subsets with bright band signature (DRW stratiform, BBY-BB, and CZD-BB), and black diamonds the probability for subsets without a bright band signature (DRW convective, BBY-NBB, and CZD-NBB). The shaded regions indicate different skewness classes.
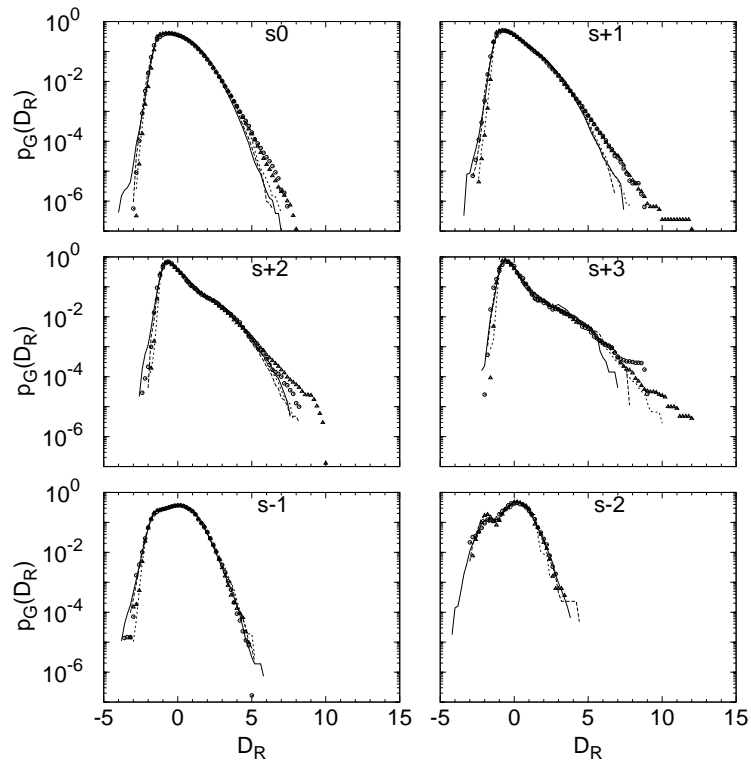
Fig. 2. $p_G(D_R)$ for skewness classes subsets obtained from the entire DRW database (solid line), the BBY-BB database (long dashed line), the CZD-BB databases (short dashed line), the BBY-NBB database (circles), and the CZD-NBB database (triangles). The label on the top of each panel indicates the skewness class: s0, s+1, s+2, s+3, s-1, and s-2.
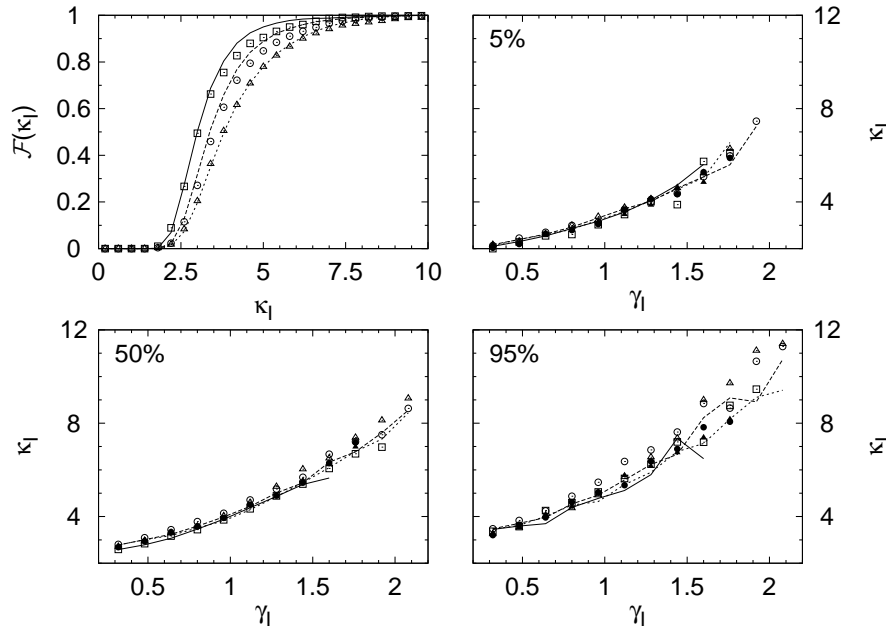
Fig. 3. Distribution of kurtosis and skewness-kurtosis relations. The top-left panel reports the cumulative distribution functions $\mathcal{F}(\kappa_l)$ of the kurtosis. The other three panels give the 5 % (top-right), 50 % (down-left), and 95 % (down-right) percentile of kurtosis in 0.16 width bin of skewness. The solid line represents DRW-BB database, long dashed line the BBY-BB database, short dashed line the CZD-BB database, the squares the DRW-NBB, the circles the BBY-NBB database, and triangles the CZD-NBB database.

Title Page

Abstract | Introduction

Conclusions | References
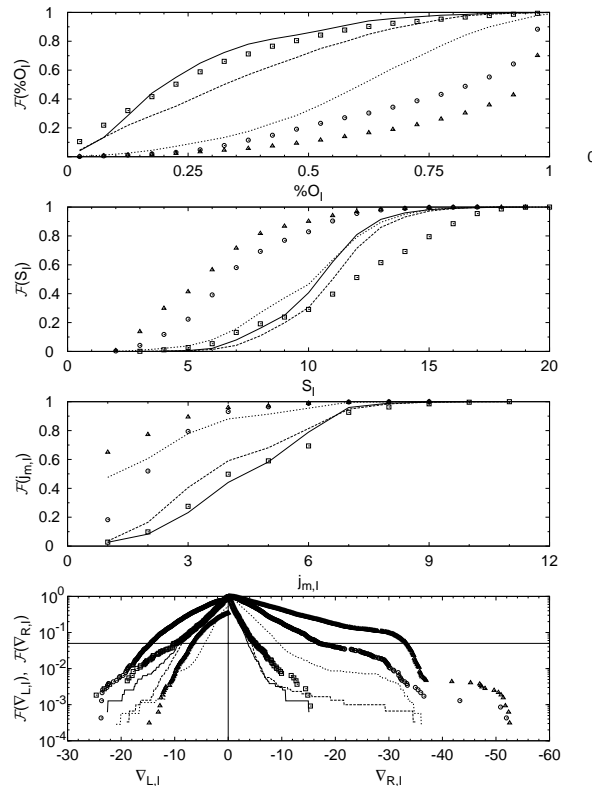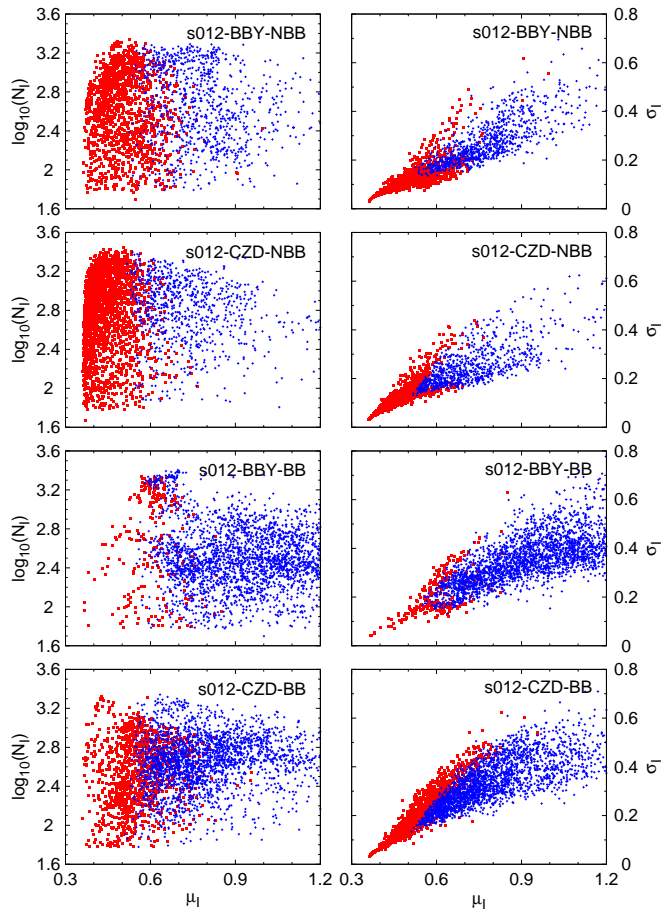
Tables | Figures

|◄ | ►|

◄ | ►

Back | Close

Full Screen / Esc

Printer-friendly Version

Interactive Discussion

Fig. 4. Cumulative density functions of the following variables: the percentage occupancy $\%O_l$ (upper panel), the class span S_l (second panel from the top), the disdrometer diameter class the maximum density $j_{m,l}$ (third panel from the top), the left and right gradients $\nabla_{L,l}$ and $\nabla_{R,l}$ of the probability density around the maximum value (lower panel). The solid line represents DRW-BB database, long dashed line the BBY-BB database, short dashed line the CZD-BB database, the squares the DRW-NBB, the circles the BBY-NBB database, and triangles the CZD-NBB database. The horizontal solid line indicates the 5 % probability level.

HESSD

8, 8101–8130, 2011

Comparison of drop size distributions

M. Ignaccolo and C. De Michele

Title Page

Abstract | Introduction

Conclusions | References

Tables | Figures

|◄ | ►|

◄ | ►

Back | Close

Full Screen / Esc

Printer-friendly Version

Interactive Discussion

Fig. 5. Steep (red squares) vs not-steep (blue crosses) portions, of BBY-NBB and CZD-NBB (the first four upper panels) and BBY-BB, CZD-BB (the four lower panels), both in the $\mu_l \log_{10}(N_l)$ plane (left panels), and in the $\mu_l \sigma_l$ plane (right panels).

Title Page

Abstract | Introduction

Conclusions | References

Tables | Figures

|◀ | ▶|

◀ | ▶

Back | Close
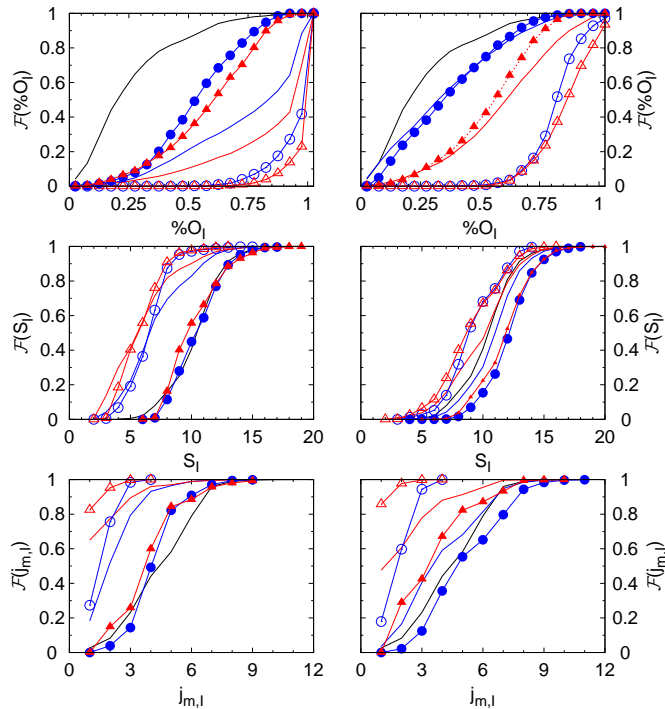
Full Screen / Esc

Printer-friendly Version

Interactive Discussion
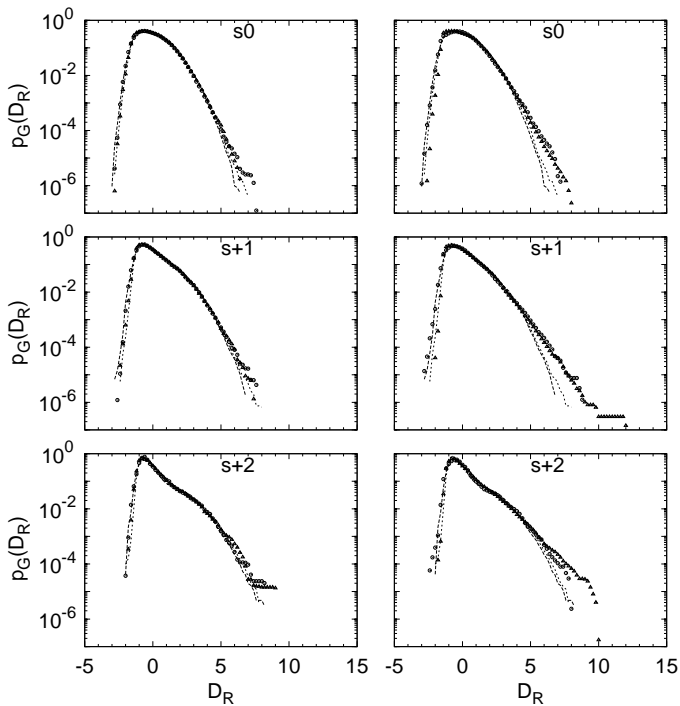
Fig. 6. $p_G(D_R)$ for the skewness classes s0, s+1, and s+2 of not-steep (left panels) and steep (right panels) portions of the s012-BBY-NBB (circles) and s012-CZD-NBB (triangles) data sets, together with the corresponding densities for BBY-BB (long dashed line), CZD-BB (short dashed line).

Fig. 7. Cumulative density functions of the following variables: the percentage occupancy %O_I (top panels), the class span S_I (middle panels), and the disdrometer diameter class the maximum density $J_{m,I}$ (bottom panels). The left (right) column refers to NBB (BB) data sets: s012-BBY-NBB (s012-BBY-BB) solid blue line, s012-CZD-NBB (s012-CZD-BB) solid red line, steep subset of s012-BBY-NBB (s012-BBY-BB) solid blue line and empty blue circles, steep subset of s012-CZDNBB (s012-CZD-BB) solid red line and empty red triangles, not-steep subset of s012-BBY-NBB (s012-BBY-BB) solid blue line and blue filled circles, and not-steep subset of s012-CZD-NBB (s012- CZD-BB) solid red line and red filled triangles. Finally, the solid black line referes, in all panel, to the s012-DRW stratiform data set.

Title Page

Abstract | Introduction

Conclusions | References

Tables | Figures

|◀ | ▶|

◀ | ▶

Back | Close

Full Screen / Esc

Printer-friendly Version

Interactive Discussion